Determination of the intergrain critical-current distribution for polycrystalline (Tl,Pb)(Ba,Sr)$_2$Ca$_2$Cu$_3$O$_y$ superconductors from ac-susceptibility data

Osvaldo F. Schilling,* Katsuzo Aihara,† Atsuko Soeta, Tomoichi Kamo, and Shin-pei Matsuda
Hitachi Research Laboratory, Hitachi Ltd., Superconductivity Research Center, 4026 Kuji-cho, Hitachi-shi, Ibaraki-ken 319-12, Japan
(Received 14 July 1992)

The intergrain critical-current-density (J_{ci}) distribution and intergranular volume fraction of ceramic superconductors were determined from ac-susceptibility measurements. The sample was melt-treated polycrystalline (Tl,Pb)(Ba,Sr)$_2$Ca$_2$Cu$_3$O$_y$ [Tl (1:2:2:3)] high-T_c ($\sim$119 K in zero field) superconductor for fields up to 80 K Oe and temperatures between 30 K and T_c. Experimental conditions were chosen so that the data could be analyzed with Bean's critical-state model associated with an extended version of the effective-medium model for the material's magnetic-shielding properties. Within this context equations relating the statistical distribution of intergrain critical currents in the sample with the measured susceptibility were derived.

I. INTRODUCTION

During the past three decades dc and ac magnetization (M) and susceptibility (χ) measurements have become a standard tool for the evaluation of transport properties of superconductors. The concept of a critical state and its use in the interpretation of ac magnetization data in terms of a critical-current density (J_c) were introduced by Bean.[1] In the early 1970s, ac flux profile techniques were introduced by Campbell[2] and Rollins, Küpfer, and Gey[3] with the same purpose. For homogeneous materials, flux profile techniques have the advantage of being independent of any particular version of the critical-state model, since the pinning force may be directly evaluated from the flux profile as a function of distance from the sample surface. With the advent of high-temperature superconductors, however, this advantage has been lost in view of the heterogeneous microstructure and magnetic properties of polycrystalline samples. In their analysis of the application of the flux profile technique to ceramic superconductors, Küpfer *et al.*[4] gave an interpretation of the data which required determination of the dependence of the average volume fraction of intergranular material upon the position corresponding to the change of slope in the profile. It is clear that determination of such a dependence can only be roughly made, in view of the irregular shape of the grains and the heterogeneous properties of the intergrain material. The flux profile technique as it is applied nowadays gives no detailed information about the actual distribution of intergranular transport properties of the samples. It appears that knowledge of such a distribution as a function of field and temperature would be of great interest for researchers involved in materials manufacture.

Susceptibility data for polycrystalline samples are complicated to analyze quantitatively. The fraction of intergranular material, shape, size, and demagnetization factors of the sample and grains, anisotropy of current flow inside and between grains, flux-pinning properties of the grains and intergrain material, and volumetric distributions of superconducting parameters and coupling properties between grains are all primary factors that influence susceptibility data. In order to decrease the degree of complexity involved the problem should be approached using the most favorable experimental conditions to avoid becoming overwhelmed by the excess of variables and fitting parameters needed to interpret the data. Particularly complex situations, as far as data interpretation is concerned, arise for dc fields (represented as H) on the order of the ac ripple field (with maximum amplitude represented by h) or smaller, or at temperatures (T) and dc fields surrounding the irreversibility line for weak-pinning materials. In such cases the critical currents are dependent not only upon the dc field, but also on position and the ac ripple field amplitude, and flux-creep effects, difficult to describe in a precise way, sometimes must be taken into account. These difficulties prevent an unequivocal analysis of the data since many assumptions are necessary. To keep assumptions to a minimum, as well as to determine as many as possible of the necessary parameters from experiment, careful choice of the experimental conditions is required.

In this work the intergranular critical-current-density distribution function and intergranular volume fraction of a polycrystalline (Tl,Pb), (Ba,Sr)$_2$Ca$_2$Cu$_3$O$_y$ [T1(1:2:2:3)] superconductor sample were determined from standard ac-susceptibility measurement techniques. Based on the restrictions outlined in the previous paragraph, the measurement conditions were chosen with $H \gg h$ in all cases. As long as the dc field H is kept constant during a set of experiments, its magnitude is expected to determine the value of the intragrain and intergrain critical-current densities (J_{cg} and J_{ci}, respectively), as in the original Bean experiment.[1]

The demagnetization factor for the prism-shaped specimen studied is about 10%, but for simplicity demagnetization corrections were neglected in the analysis. Under such conditions the Bean critical-state model equations for a long cylinder in an axial field were assumed to be applicable. Although the specimen may be modeled as a long cylinder for calculational purposes, the superconductor grain contribution to the measured susceptibility

depends strongly on their shape, especially when these grains are sparsely distributed.[5,6] Most papers have followed Clem's[7] approach of taking the grains as long cylinders with a zero demagnetization factor. In the analysis of the present data it became clear, however, that such an assumption, as expected,[6] did not remain true as the superconductor volume fraction (f) decreased at high temperatures. In order to obtain a quantitative fit for high-temperature data (around and above the peak in the plot of susceptibility versus temperature) some correction was therefore needed. A better fit to the experimental data was obtained by assuming the grains were cylinders in a *transverse* field instead. For such an orientation the demagnetization factor for elongated grains saturates quite rapidly at about $\frac{1}{2}$ as the length becomes greater than the diameter. At lower temperatures the grains were assumed as closely packed, and no demagnetization correction is needed as a result of pole cancellation on contiguous neighboring grain surfaces.[6]

Since the specimen is not homogeneous, with the presence of normal phases and weak links between superconducting grains, the material must be modeled as an "effective medium." The effective-medium concept has been made quantitative for ceramic superconductors by Clem,[7] and later by several others.[8–10] The measured susceptibility is then regarded as a linear combination of the intergrain and intragrain contributions. In this approximation, which is designated the *conventional* model, the medium consists of just two phases, one of them normal with *uniform* transport properties, and the other, a superconductor. Such a hypothesis, however, has limited validity if the transport properties assume a wide range of values. In order to determine such a distribution from the data, an *extended* effective medium model was developed in this paper. The measured intergrain susceptibility then results from an average taken over the distribution of intergrain transport properties.

Section II describes the characteristics of the sample and the measurement technique. Section III presents details of the conventional and extended versions of the effective-medium model. Section IV presents the experimental results and their discussion.

II. MATERIALS AND METHODS

The measurements were carried out for a melt-treated multiphase (Tl/Pb)-(Sr/Ba)-Ca-Cu-O bulk sample, with nominal atomic ratio of (0.5/0.5)-(1.6/0.4)-2-3 [Tl-(1:2:2:3)], and dimensions $1\times1\times5$ mm.[3] The manufacturing conditions have been described elsewhere.[11] X-ray analysis showed that the major constituents were Tl-(1:2:2:3), Tl-(1:2:1:2), and $BaPbO_3$, after partial melting and annealing. Further scanning-electron-microscopy–energy-dispersive -x-ray (SEM-EDX) analysis revealed the formation of $(Ca, Sr)_2CuO_3$ after the partial melt. The grain size of the Tl-(1:2:2:3) phase was 50–200 μm. A typical micrograph displaying features of the microstructure is shown in Fig. 1.

For the ac susceptibility measurements an HP-4192A impedance analyzer was utilized. A probing ac ripple field of maximum amplitude h [$h(\mathrm{ac})=h\cos(2\pi\nu t)$] adjustable between 0.04 and 4.2 Oe was imposed onto the sample. The frequency adopted in all measurements was $\nu=500$ Hz. dc fields applied parallel to the long axis of the sample could be set between 0 and 80 kOe, either by using a low-field bobbin immersed in liquid nitrogen, or by using a high-field, Hitachi-made superconducting magnet.

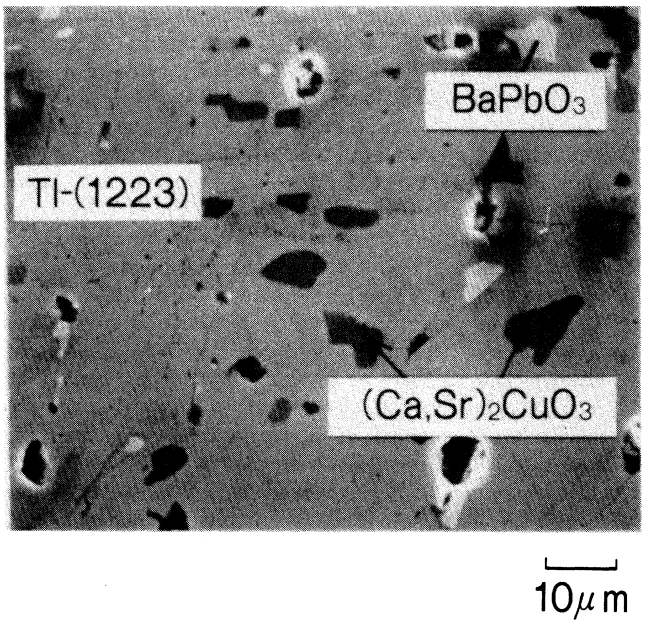

FIG. 1. SEM micrograph showing a large Tl-(1:2:2:3) grain with other phases embedded in it.

Since the kind of equipment used here is commonly available in other laboratories, it was thought beneficial to include a more detailed discussion about the relation between the output of the impedance analyzer and $\chi=\chi'+j\chi''$. The impedance analyzer measures the voltage (V) in a pickup coil (A) with the sample inside and compares it with the voltage in an empty cancel coil (B) wound above the pickup coil along the probe rod. The equipment basically yields two sets of data. It gives the gain "$A-B$" as ("mod" denotes modulus)

$$20\log_{10}(\mathrm{mod}\{V_A\}/\mathrm{mod}\{V_B\}),$$

and the phase angle between the signals A and B,

$$\phi=a\tan[-g4\pi\chi''/(1+g4\pi\chi')],$$

where

$$\mathrm{mod}\{V_A\}/\mathrm{mod}\{V_B\}=[(1+g4\pi\chi')^2+(g4\pi\chi'')^2]^{1/2}$$

and g is an experimentally determined parameter proportional to the ratio between the coils mutual (with sample) and self-inductances, and proportional also to the ratio between h and the current in the coil.[12] For the present experiments $g=0.0384$ was determined from the full scale of $A-B=-0.34$, corresponding to assuming $4\pi\chi'=-1$ and $4\pi\chi''=0$ at low T in zero field. (No demagnetization corrections were included in χ.) There-

fore, by neglecting small corrections dependent on $g\chi'$ and taking $\cos(\phi)\approx 1$, for the present conditions $4\pi\chi''=-26\tan(\phi)$ and $4\pi\chi'=3(A-B)$, with $\tan(\phi)\approx\phi$ since the angle ϕ was always very small.

The susceptibility terms χ' and χ'' are the respective coefficients in cosine and sine of the fundamental harmonic ($\nu=500$ Hz) in the Fourier expansion of M/h (for full expressions see Ref. 6). In the actual fits to the experimental data, simplified expressions for χ' for cylinders at $h^*<h$ (see Sec. III A) were adopted (taking the same approach as Gotoh *et al.* did for slabs.[13]) In this approach χ' is taken as the ratio $M(t)/h$ at the end of the first quarter cycle of the ripple field sweep. The complete expression requires the integration of $M(t)\cos(2\pi\nu t)$ over the whole cycle. In the absence of other sources of error the effects in the overall fit to the data resulting from this assumption are relevant only at very low $|\chi'|$, a situation that corresponds to high temperatures. However, under such conditions the necessity of intragrain-related corrections ends up compensating for the effects of the simplification. The use of simplified expressions is advantageous since it leads to linearization of the expression for χ' for $h>h^*$ [see Eqs. (2) and (4)], allowing the straightforward determination of the intergrain critical-currents distribution from the derivatives of $4\pi\chi'$, as shown in Sec. III B. This also permits the analytical integration of Eq. (4), which would be impossible with the complex full expressions[6] for $h>h^*$; thus the fitting procedure is facilitated.

Two different kinds of experiments were carried out, as described below. Type (i): These were carried out under field-cooled (FC) conditions. The field H is applied above T_c, and the sample is cooled to ≈ 20 K. The χ data are then recorded while slowly heating the sample up to T_c. The analysis covers data obtained at $H=10$ and 80 kOe, for $h=0.21$, 1.05, 2.1, and 4.2 Oe for each dc field. Type (ii): These were carried out under zero-field-cooled conditions (ZFC) by cooling without a field down to 77 K, applying H and ramping h at constant $T=77$ K from 0.04 up to 4.2 Oe (h sweep experiments).

The fraction f and the J_c's can be determined at a given temperature from the data of experiments (ii), interpreted either by the conventional or extended effective-medium models. A single experiment of type (i) does not reveal much about the parameters of the model since the temperature dependence of the parameters is not known. However, if several experiments of type (i) are carried out adopting a different h for each run, the data obtained can effectively simulate a sequence of experiments (ii) yielding the fraction f and the J_c's in the whole range of temperature at a given H. By choosing several temperatures on the χ' versus T plots, four values of $\chi'(h)$ are obtained at each T and H. These data can be fit by the Bean model associated either with the conventional effective-medium model, or with the extended version, as described in the next section, to obtain the parameters f and J_{ci}. The extended model allows determination of the intergrain critical-current distribution at each T and H from the χ' and χ'' versus h plots. This avoids the necessity of guessing such temperature dependences from particular flux pinning or flux-creep models.

III. EFFECTIVE-MEDIUM ANALYSIS

A. Conventional effective-medium model

As discussed in Sec. I, the sample may be regarded as an infinite cylinder in an axial field. The sample is assumed to contain a volume fraction f of superconductor grains and inclusions within them. In the conventional approach the complementary $f_n=1-f$ fraction of intergrain material has uniform properties. The intergrain critical-current density J_{ci}, which is actually distributed over a broad range of values, shields the bulk of the specimen against the penetration of the ac field along the intergranular regions. The intragrain current density J_{cg} shields the bulk of the grains against the ac field penetration. The magnitudes of both current systems are effectively imposed by the much greater dc field H. Following Refs. 7–9, it is possible to write

$$4\pi\chi=(1-\mu)4\pi\chi_g+\mu 4\pi\chi_i\ , \tag{1}$$

where χ, χ_g, and χ_i are the sample, intragrain, and intergrain complex susceptibilities, respectively, and μ is the effective permeability of the specimen. The high value of the Ginzburg-Landau parameter κ makes $B\approx H$ (cgs units) in view of the small value of the reversible magnetization which is inversely proportional to κ^2, so that μ does not need further correction of the form dH/dB, which is relevant for conventional superconductors.[14] The permeability μ may be taken as equal to f_n since the grain size is large compared to the London penetration depth at most temperatures.[7]

As already discussed, the Bean model for cylinders is expected to apply in such conditions. The relevant expressions for χ' and χ'' are (Refs. 6 and 13 for slabs)

$$4\pi\chi'=-1+5h/(\pi DJ_c)-\tfrac{1}{3}[5h/(\pi DJ_c)]^2 \quad \text{for } h\le h^*\ , \tag{2a}$$

$$4\pi\chi'=-\tfrac{1}{3}[\pi J_c D/(5h)] \quad \text{for } h\ge h^*\ , \tag{2b}$$

$$4\pi\chi''=\{4[5h/(\pi J_c D)]-2[5h/(\pi J_c D)]^2\}/(3\pi) \quad \text{for } h\le h^*\ , \tag{3a}$$

$$4\pi\chi''=\{4[\pi J_c D/(5h)]-2[\pi J_c D/(5h)]^2\}/(3\pi) \quad \text{for } h\ge h^*\ . \tag{3b}$$

Here D is either the diameter of the sample or of the intragrain current loops, J_c is either the intergrain or intragrain critical-current density, and $h^*=\pi J_C D/5$ is the field amplitude corresponding to full penetration either of the sample or loops. For long cylinders in a transverse field[6] the only correction needed is to multiply Eqs. (2) and (3) by 2, to account for the demagnetization factor $\frac{1}{2}$. Practical units are used, with the current densities in A/cm^2, magnetic field in Oe, and length in cm. In practice, the high values of J_{cg} make Eqs. (2) and (3) irrelevant for the grains for most $T<T_c$, since $\chi_g''\approx 0$ and $4\pi\chi_g'\approx -1$ in such conditions.

Attempts to fit this model to experiments have shown that the conventional approach has very limited applica-

bility since it requires assuming that the broad distribution of the J_{ci} values is represented by a δ function. The J_c figures obtained may be misleading since they are not, in general, related to the actual distribution, but instead to an idealized sharp distribution. In the next subsection an extended model is developed in which the existence of a distribution of intergrain properties is taken into consideration.

B. Extended effective-medium model

Here a model is introduced that accounts for a distribution of intergrain critical-current densities J_{ci}, or, in other terms, of full penetration fields $h^*=\pi J_{ci}D/5$, for a sample of diameter D. At high temperatures the introduction of an intragrain current density distribution is also necessary.

A long cylindrical sample is divided into a series of imaginary slices cut perpendicularly to the long axis, with each slice having a different h^* within a distribution $N(h^*)$ in units of Oe^{-1}. The thickness of each slice can be considered as the average grain size. In order to apply the Bean model the properties within each of the sections are considered homogeneous.[15] At low temperatures the intragrain J_{cg} is very high, so that full grain shielding is assumed over a wide range of conditions. Equation (1) is thus rewritten in the form

$$4\pi\chi'=\int_h^{h_{\max}}N(x)\left[-1+\frac{h}{x}-\frac{h^2}{3x^2}\right]dx - \int_{h_{\min}}^{h}N(x)\frac{x}{3h}dx - \left[1-\int_{h_{\min}}^{h_{\max}}N(x)dx\right], \tag{4}$$

$$4\pi\chi''=\frac{1}{3\pi}\left[\int_{h_{\min}}^{h}N(x)\left[\frac{4x}{h}-\frac{2x^2}{h^2}\right]dx + \int_h^{h_{\max}}N(x)\left[\frac{4h}{x}-\frac{2h^2}{x^2}\right]dx\right]. \tag{5}$$

The integration over x accounts for contributions of the whole distribution of h^* to the measured χ. The parameters $h_{\min}$ and $h_{\max}$ denote the lower and upper limits of the distribution, respectively. Equations (4) and (5) assume $h_{\min}<h<h_{\max}$. If $h<h_{\min}$, there is no full field penetration down to the center anywhere in the sample and only in integrals from h (replaced by $h_{\min}$) to $h_{\max}$ remain. If $h>h_{\max}$ the ripple field can reach the center of the sample everywhere along the axis and only the integrals from $h_{\min}$ to h (replaced by $h_{\max}$) remain. In Eqs. (4) and (5) the expressions for $4\pi\chi'$ and $4\pi\chi''$ in Eqs. (2) and (3) are adopted. The last term on the far right in Eq. (4) is the intragrain susceptibility contribution, and the integral of $N(x)$ between the limits of the distribution gives the total fraction of intergrain material f_n, which has been included as part of N. $N(h)$ may thus be obtained by successive approximations so that both the χ' and χ'' data may be fitted.

At high temperatures the assumption of very high h_g^* ($=\pi J_{cg}D_g/5$) does not remain valid for the grains. In this case the existence of a distribution of intragrain critical-current densities $N_g(h_g^*)$ must be accounted for, since it overlaps $N(h^*)$. In order to correct Eq. (4) for such overlap the last term on the right must be replaced by

$$4\pi\chi_g'=2\left[\int_h^{h_{g\text{-max}}}N_g(x)\left[-1+\frac{h}{x}-\frac{h^2}{3x^2}\right]dx - \int_{h_{g\text{-min}}}^{h}N_g(x)\frac{x}{3h}dx\right], \tag{6}$$

and Eq. (5) must include the intragrain χ'' given by

$$4\pi\chi_g''=\frac{2}{3\pi}\left[\int_{h_{g\text{-min}}}^{h}N_g(x)\left[\frac{4x}{h}-\frac{2x^2}{h^2}\right]dx + \int_h^{h_{g\text{-max}}}N_g(x)\left[\frac{4h}{x}-\frac{2h^2}{x^2}\right]dx\right]. \tag{7}$$

Here $h_{g\text{-min}}$ and $h_{g\text{-max}}$ are the limits of the N_g distribution. The major effect of these intragrain terms is the addition of a tail to the N distribution. In Eqs. (6) and (7), h is the maximum amplitude of the ac internal field h(ac) at a grain surface. This should differ from the applied h by a factor $-n\times 4\pi M(h)$, where n is the demagnetization factor of the sample.[16] Such a small correction has been neglected in the analysis since its effects do not seem to be strong enough to influence the measured data in a visible way.

At given H and T the measured susceptibility is only a function of h. It is thus possible to deduce an analytic expression for $N(h)$ at low temperatures by repeatedly taking partial derivatives of Eq. (4) to obtain

$$N(h)=2h^2\frac{\partial^3(4\pi\chi')}{\partial h^3}+\frac{h^3}{2}\frac{\partial^4(4\pi\chi')}{\partial h^4}. \tag{8}$$

Equation (8) gives the distribution of intergrain critical-current densities [since $J_{ci}=5h/(\pi D)$] obtained from experimentally determined susceptibility data for full grain shielding conditions and low f_n. In particular, $N(0)=0$ if the distribution goes down to $h_{\min}=0$. Since the method is based upon susceptibility measurements and a slice with $h^*=0$ gives no contribution since its volume is completely permeable, the method gives no information about sections of the sample containing no interconnected superconducting parts. This might result in error if the volume of fully permeable material increases strongly with T or H since the calibration is done at low T and zero field. However, there is no evidence for the necessity of corrections in g; it is taken as constant for all the measurement conditions.

The derivatives needed in Eq. (8) may be obtained by fitting the χ' data and taking the derivatives of the fitting equation expression. However, since many different expressions may produce good fits to χ', in order to get the best $N(h)$ the first approximation for the distribution must then be inserted into Eq. (5) to check whether it can fit the χ'' data as well. Once corrections are made the new $N(h)$ is reinserted into Eq. (4) and the new theoretical χ' are compared with the χ' data. Proceeding in the

iterations, the method should converge in a few steps yielding an optimized distribution function consistent both with χ' and χ''.

All the results from the low-T data analysis reported in Sec. IV assumed a distribution function of the form $N(h^*)=f_n k^2 h^* \times \exp(-kh^*)$, with k and $f_n \geq$ zero being obtained from the fits, with $h_{\min}=0$ and infinite $h_{\max}$. When intragrain corrections were necessary, a similar expression for $N_g(h^*)$ was assumed, with the form $(1-f_n)k_g^2 h^* \times \exp(-k_g h^*)$. It was verified that other expressions with slower high-h decays may be adopted for N, but these require taking some cutoff $h_{\max}$ beyond the present experimental range, thereby introducing a further fitting parameter that can be avoided by assuming exponential decay.

IV. EXPERIMENTAL RESULTS AND DISCUSSION

A. Interpretation of susceptibility data in terms of distributions of current density

Figure 2 shows some of the plots of χ' and χ'' versus h for h-sweep experiments carried out at 77 K and H between 26 and 500 Oe. The fits provided by the extended effective-medium model are also shown. Figure 3 displays the corresponding distribution functions for five different values of H. The h^* scale may be regarded as a J_{ci} scale by noting that, for $D=0.1$ cm, $h^*=1$ Oe corresponds to $J_{ci}=16$ A/cm^2. It appears that as H is increased the distribution gets more concentrated at low h^*, with f_n increasing from 0.3 to 0.39. The distributions, however, may not be very precisely determined at high h^* due to the maximum $h=4.2$ Oe not allowing measurements at higher fields. Therefore, the possibility of a long low-N tail cannot be eliminated. Then there is no need for inclusion of intragrain-related corrections in order to get good fits, since h_g^* for the grains appears to be quite high at 77 K and low H.

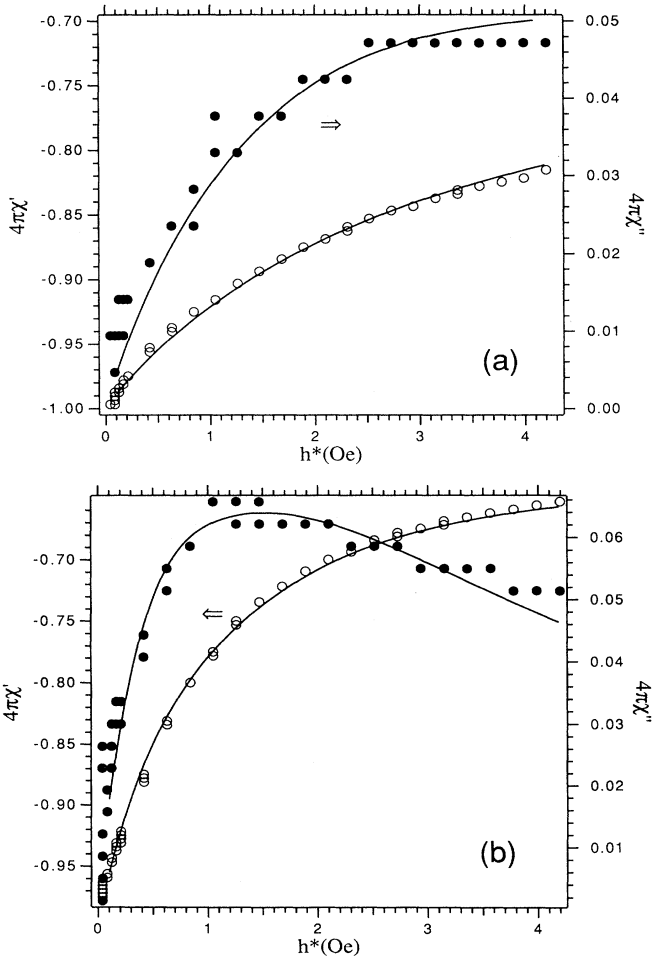

FIG. 2. χ' and χ'' data and fits to the data from the extended effective-medium model for (a) $H=26$ Oe, $T=77$ K; and (b) $H=500$ Oe, $T=77$ K.

Experiments of type (i) were carried out for $h=0.21$, 1.05, 2.1, and 4.2 Oe, at $H=10$ and 80 kOe. Figure 4 shows the χ' and χ'' versus T data for $H=10$ kOe. The data in Fig. 4 may be adopted to obtain the values of $N(h^*)$ in the whole range of T by choosing several temperatures and fitting each set of four points to Eqs. (4) and (5). To illustrate the method, Figs. 5 and 6 present fits and distributions for $T=40$, 60, 77, and 100 K and $H=10$ kOe. For the 77-K case an alternative distribution of the form $h/(a+h^2)$ was also tested. It can provide a good fit to the χ' and χ'' data and it is also displayed in the figure. This latter distribution has a long low-N tail and a cutoff $h_{\max}$ of 5.3 Oe was adopted in the integrations. The fit to the 100-K data required the intragrain corrections be made. This allowed a very good description of the χ'' data, although the corresponding χ' fit was not so precise.

The degree of accuracy in the fitting procedure clearly depends on the form of the distribution function adopted. The same function $h/(a+h^2)$ used in the alternative fit to the 77-K, 10-kOe data was tried at higher T but problems arose with the convergence of the integral of

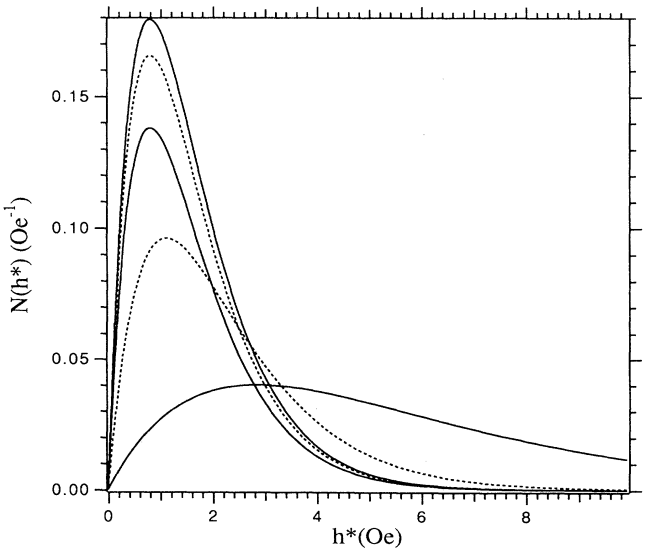

FIG. 3. Distributions calculated for the fits to the ZFC set of experiments at 77 K. From top: $H=500$, 200, 76, 50, and 26 Oe.

$N(h)dh$, so that a reliable value of f_n was not obtained from such a fit. However, when the distribution was spread over a relatively wide range, the susceptibility calculations were less sensitive to uncertainties in the distribution form.

Figures 7 and 8 show fits and distributions for 60, 80, and 84 K for $H=80$ kOe. The 84-K data were already beyond the χ'' peak for $h=0.21$ Oe. Both fits to the 80- and 84-K data required the intragrain-related corrections. There are significant variations of the distributions in this 24-K temperature interval. f_n increases from 0.55 at 60 K to 0.63 at 80 K and 0.92 at 84 K, showing great sensitivity to the temperature of the weak-link distribution and transport properties near the χ'' peak.

In general, the distribution dependence upon T resembles the dependence upon H in the sense that at low T (low H) the distributions are much broader than at the higher T (H) tested. An interesting point seen from the determination of these distributions is that for $T=77$ K and 10 kOe, f_n is still about 45% [49% if the $h/(a+h^2)$ curve is adopted], i.e., not so much greater compared to the 31% value for $H=26$ Oe. This means that for a wide range of field at 77 K the weak-link fraction is not very field sensitive.

The main results from analysis of the data are displayed in Table I. For each intergrain distribution it was possible to calculate an average $\langle J_{ci}\rangle = 32/k$ A/cm^2, for $D=0.1$ cm. Transport current-density measurements (unpublished) carried out in similar samples at 77 K were found to give results that may lay either above or below these averages $\langle J_{ci}\rangle$. At 77 K the $\langle J_{ci}\rangle$ data drop faster with the field than do the transport J_c obtained from a 1-μV/cm criterion applied to V versus I curves, reaching a plateau of similar magnitude beyond 10 kOe.

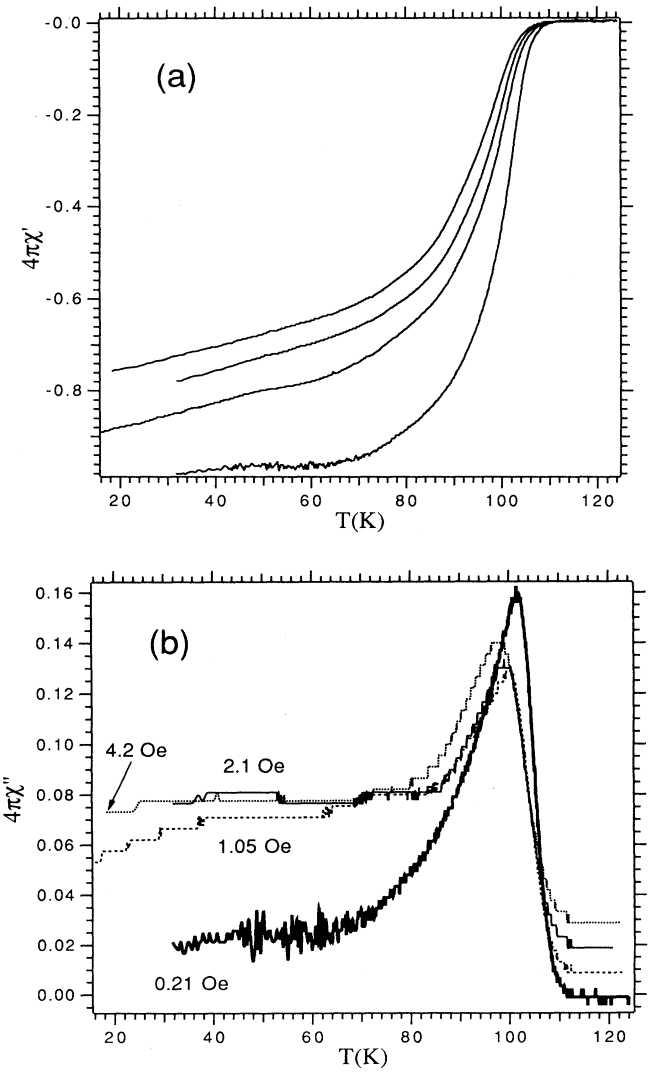

FIG. 4. (a) χ' vs T plots for the FC experiments at $H=10$ kOe. From top: $h=4.2$, 2.1, 1.05, and 0.21 Oe. (b) χ'' vs T plots for $H=10$ kOe. The baselines are displaced vertically for clarity.

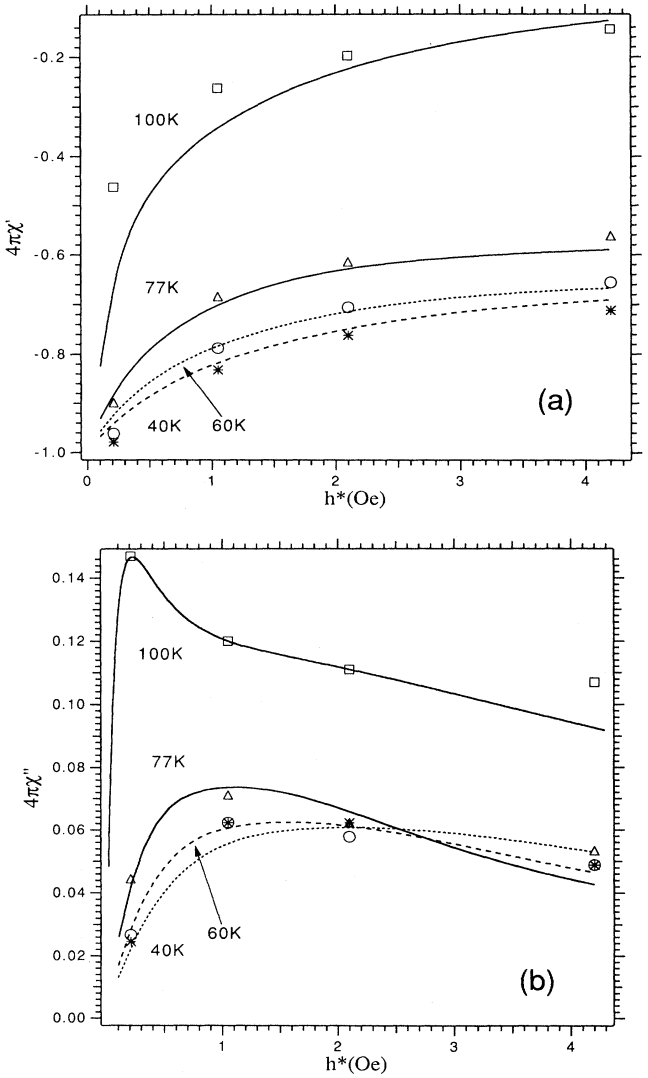

FIG. 5. (a) χ' vs h and fits for several temperatures at $H=10$ kOe: squares, 100 K; triangles, 77 K; circles, 60 K; and stars, 40 K. (b) Corresponding χ'' vs h plots and fits. $T=100$ K corresponds to the peak of the χ'' data for $h=0.21$ Oe.

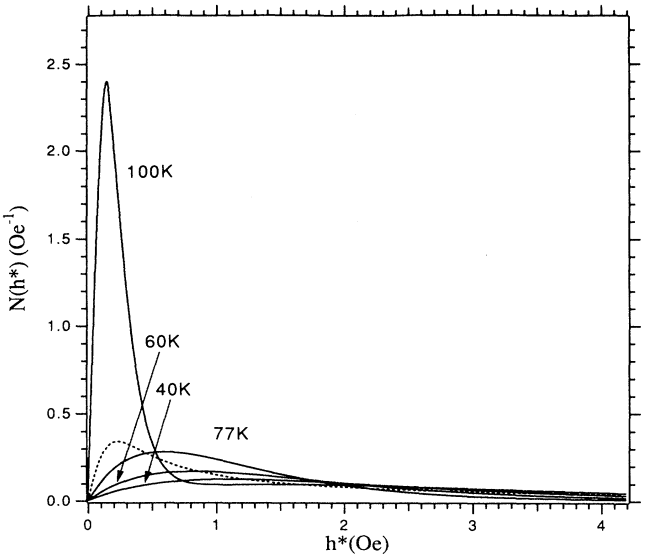

FIG. 6. Distributions corresponding to the fits in Fig. 5. The dotted line is an alternative distribution for $T=77$ K, with $f_n=49\%$ (see text).

B. Comparison with distributions obtained from transport measurements

Several papers have presented calculations of current-density distributions obtained from transport current measurements rather than from susceptibility measurements. Irie, Tsujioka, and Chiba[17] have recently proposed a model in which a distribution of critical-current densities may be obtained from the second derivative of the V versus I curves. Such a model postulates that the rupture probability of flux line lattice pins may be described with a Weibull function. Alternative models have been proposed by Griessen,[18] who obtained a distribution of pinning energies from the V versus I plots, and by Wördenweber and Abd-El-Hamed.[19] These latter authors assume that resistive behavior in films arises when parts of the flux line lattice shear through weak-pinning channels in the material. Depending on the relation between the current density J and the J_c of a channel its contribution to the electric field is either zero (for $J<J_c$) or $\rho_f(J-J_c)$, with ρ_f denoting the flux-flow resistivity. The V versus I curves are thus fitted by assuming a distribution of J_c's for the channels.

By analyzing transport data available for Tl-(1:2:2:3) samples similar to the one used in the susceptibility experiments, it appeared that J_c distributions obtained from ac-susceptibility and direct transport measurements differed significantly from each other. The V versus I curves display a sharp increase in V as I reaches a certain value I_c, usually close to the 1 μV/cm condition. By taking the second derivative of the V versus I curve as in Ref. 17, the resulting distribution is approximately zero below $J_{c,\min}=I_c/A$, where A is the sample cross-sectional area. This was clearly inconsistent with the distributions obtained from the susceptibility data, which can only be fit by assuming that a high proportion of junctions has low J_{ci}. The reason for such discrepancy is that the calculation of N from the second derivative of V involves the assumption that the resistive elements (e.g., weak-pinning channels, grain boundaries) are arranged in a simple *series* array. This may be better understood by solving the differential equation $d^2E/dJ^2=\rho_f N(J)$, to obtain

$$E=\int_{J_{c\text{-min}}}^{J}\rho_f(J-J_c)N(J_c)dJ_c\ . \tag{9}$$

Equation (9) gives the electric field generated by a series array of resistive elements with J_c distributed between a $J_{c,\min}$ and a $J_{c,\max}$ that is greater than J, the externally imposed average current density. As discussed in the previous paragraph only elements with $J_c<J$ contribute to E. This model makes no provision for the possibility of current flowing round highly resistive paths through more favorable parallel paths. The series array model therefore involves a clear oversimplification of physical reality. Its main consequence, as far as the determination of $N(J)$ is concerned, is that fitting Eq. (9)

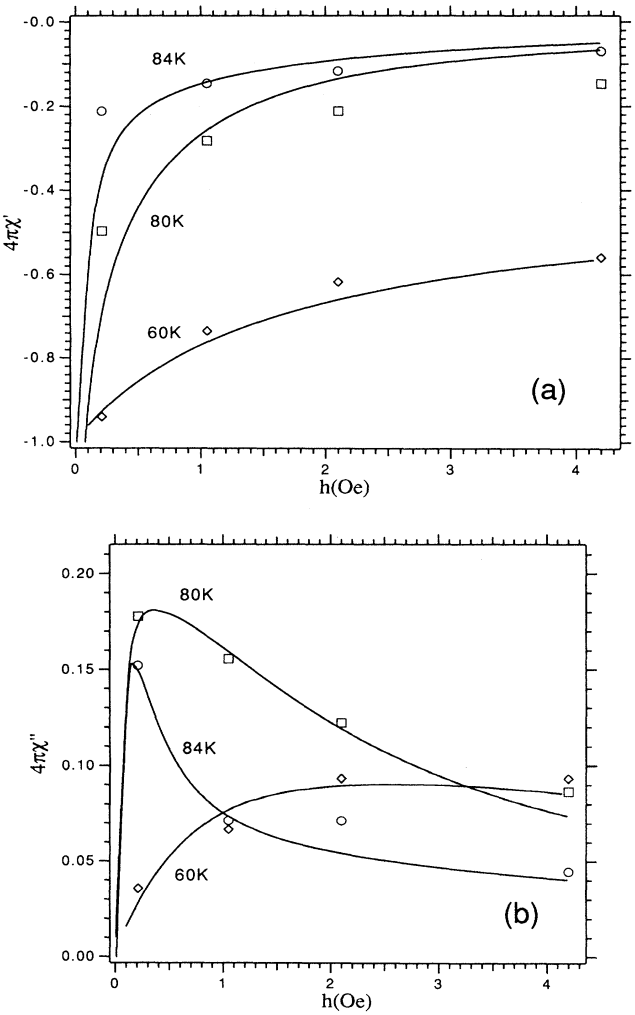

FIG. 7. (a) χ' vs h and fits for several temperatures at $H=80$ kOe: circles, 84 K; squares, 80 K; and diamonds, 60 K. (b) Corresponding χ'' vs h plots and fits.

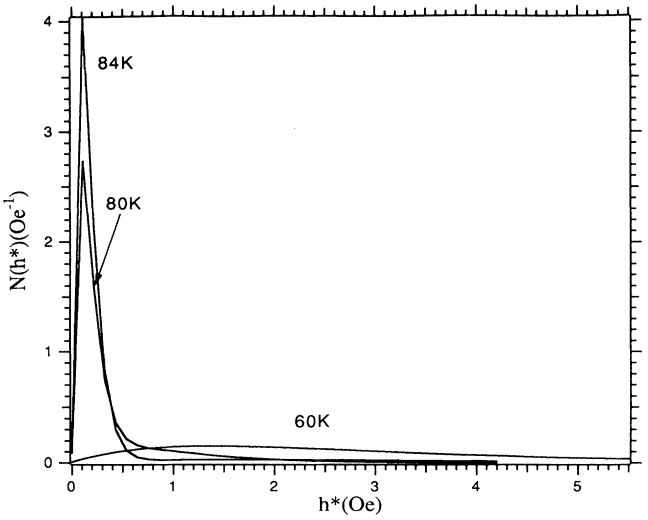

FIG. 8. Distributions corresponding to the fits of Fig. 7.

to an actual E versus J curve yields $J_{c,\min}=I_c/A$, that is, $N(J)$ ends up distorted so that low-J_c contributions are erased. Since the interpretation of the ac-susceptibility measurements proposed in this paper accounts for the actual parallel flow of shielding currents in the sample, it appears that the $N(h^*)$ calculated in the previous sections do not suffer from the same limitation.

To supplement the present work the authors have calculated realistic V versus I curves for thin polycrystalline samples based upon the knowledge of the distribution of J_c for the boundaries.[20] By assuming $N(J_c)=k^2J_c\exp(-kJ_c)$ the simulations have shown that the onset of a clear departure from the $V\approx 0$ baseline takes place for $J_c\approx 1.5/k$, so that it was shown that distributions of J_c may be found that are consistent both with direct V versus I data as well as with ac susceptibility measurements.

TABLE I. Main results of the analysis. In the lines with two k values the second one corresponds to k_g (see text). $\langle J_{ci}\rangle=32/k$ A/cm^2.

H (Oe)	T (K)	f_n (%)	k (1/Oe)	$\langle J_{ci}\rangle$ A/cm^2	Obs.
26		31	0.35	91	
50		29	0.9	36	
76	77	30	1.25	26	ZFC
200		36	1.25	26	
500		39	1.25	26	
10 000	40	37	0.9	36	
	60	38	1.2	27	
	77	45	1.7	19	
	100	75	10, 0.7	3.2	
					FC
80 000	60	55	0.72	44	
	80	63	12, 1.9	2.7	
	84	92	13, 0.6	2.6	

C. Flux-creep effects

Another interesting issue is whether or not flux creep affects the transport properties of Tl-(1:2:2:3). Apparently thermally activated depinning is negligible even at the higher temperatures and fields tested. The high-temperature χ' and χ'' data for 10 and 80 kOe are not strongly dependent on h, which might be an indication of viscous flux drag effects.[14] Nevertheless, the present analysis has been able to relate such weak h dependence to the existence of a J_c distribution, entirely within the critical state model framework. It is important to note that the dominance of flux creep would make the χ'' data reach values about 81% higher (cf. Ref. 14) than for the critical state. In a related study[21] on a $Bi_2Sr_2CaCu_2O_x$ single-crystal correction factors in the range 1.3–2 had to be applied to the measured χ'' data in order to make them compare with the calculated curves from a flux-creep model. It is very likely that such data and others of the same nature might be better interpreted by assuming a distribution of J_c's (even for crystals) and a critical state model rather than flux-creep models.

V. CONCLUSIONS

Measurements of the intergrain critical-current-density distribution have been carried out in a Tl-(1:2:2:3) sample. The method involved a combination of the effective-medium model with the Bean critical state model. At each temperature the only parameters needed for the fit were f_n and the characteristic decay range of the distribution, $1/k$. Equations relating the distribution $N(h^*)$ with the real and imaginary parts of the ac susceptibility were derived. At 77 K the *range* of h^* covered by the distribution decreased rapidly from about 10 Oe (160 A/cm^2) for $H=26$ Oe and saturated at about 3 Oe (48 A/cm^2) at high fields. At 77 K the fraction of intergrain material f_n varied from 31% at 26 Oe (ZFC conditions), to 45% at 10 kOe (FC conditions), until reaching about 90% at 80 kOe.

At high temperatures and fields the superconductor grains became isolated by thick normal grain boundaries. Under such conditions their demagnetization factors must be taken into account, and their full contribution to χ' and χ'' must be calculated in detail. These high-temperature–high-field data were fairly well described just by considering the grains as long cylinders in a transverse field, with a demagnetization factor of $\frac{1}{2}$. In all cases the sample was well represented as a long cylinder in an axial field.

By varying the temperature at 10 and 80 kOe the distributions were shown to remain concentrated below a maximum J_{ci} of ≈ 100 A/cm^2, with f_n progressively increasing as T increased. At the highest temperatures the distribution of intragrain h_g^*'s overlapped the intergrain distribution forming a long low-N tail.

In general, the method has proved capable of giving an acceptable, consistent account of both χ' and χ'' data for all conditions tested, which included most of those relevant for practical applications. The results of the present paper clearly showed that the critical-current

density in a high-T_c superconductor was distributed over a relatively wide range of values. Although attractive for its simplicity, the idea of representing such a distribution by a single number may be misleading if the statistical deviation from this average is not known. The present method provides a simple theoretical-experimental framework upon which the distributions can be determined from ac-susceptibility measurements.

ACKNOWLEDGMENT

The authors wish to thank M. Okada for valuable discussions.

*Present address: Instituto de Fisica, Unicamp, Caixa Postal 6165, Campinas, Sao Paulo 13081, Brazil.

†To whom all correspondence should be addressed.

[1]C. P. Bean, Rev. Mod. Phys. **36**, 31 (1964), note misprints in Eqs. (5) and (7).

[2]A. M. Campbell, J. Phys. C **2**, 1492 (1969).

[3]R. W. Rollins, H. Küpfer, and W. Gey, J. Appl. Phys. **45**, 5392 (1974).

[4]H. Küpfer, I. Apfelstedt, R. Flükiger, C. Keller, R. Meier-Hirmer, B. Runtsch, A. Turowski, U. Wiech, and T. Wolf, Cryogenics **29**, S268 (1989); **28**, 650 (1988).

[5]A. M. Campbell and J. E. Evetts, Adv. Phys. **21**, 199 (1972), see Sec. 3.3.4.

[6]R. B. Goldfarb, M. Lelental, and C. A. Thompson, in *Magnetic Susceptibility of Superconductors and Other Spin Systems,* edited by R. A. Hein, T. L. Francavilla, and D. H. Liebenberg (Plenum, New York, 1992).

[7]J. R. Clem, Physica C **153–155**, 50 (1988).

[8]D.-X. Chen, J. Nogués, and K. V. Rao, Cyrogenics **29**, 800 (1989); D.-X. Chen, Y. Mei, and H. L. Luo, Physica C **167**, 317 (1990); D.-X. Chen, A. Sánchez, T. Puig, L. M. Martínez, and J. S. Muñoz, *ibid.* **168**, 652 (1990).

[9]K.-H. Müller, Physica C **168**, 585 (1990); **159**, 717 (1989).

[10]T. C. Choy and A. M. Stoneham, J. Phys.: Condens. Matter **2**, 939 (1990).

[11]T. Kamo, T. Doi, A. Soeta, T. Yuasa, N. Inouie, K. Aihara, and S. Matsuda, Appl. Phys. Lett. **59**, 3186 (1991); T. Doi, M. Okada, A. Soeta, T. Yuasa, K. Aihara, T. Kamo, and S. Matsuda, Physica C **183**, 67 (1991).

[12]R. B. Goldfarb and J. V. Minervini, Rev. Sci. Instrum. **55**, 761 (1984).

[13]S. Gotoh, M. Murakami, H. Fujimoto, N. Koshizuka, and S. Tanaka, Physica C **166**, 215 (1990).

[14]J. R. Clem, R. H. Kerchner, and S. T. Sekula, Phys. Rev. B **14**, 1893 (1976).

[15]Such assumption brings in the issue of the applicability of the simple Bean model equations to each of the slices separately. Such analysis requires homogeneous transport properties within each slice and the absence of shape-related demagnetization corrections. Since the slices would be quite thin ($\approx 1\%$ of the total length of the sample) it seems reasonable to assume that the intergrain material may be considered homogeneous at least in such a fine scale, something less likely when macroscopic length scales within the sample are concerned. Further, pole cancellation at the slices bounding flat surfaces is expected to cancel demagnetization effects in neighboring slices (Ref. 6). This effect eliminates border contributions and thus the application of equations derived for the long cylindrical geometry in the analysis of the critical state in each of the slices seems justifiable.

[16]D.-X. Chen, J. A. Brug, and R. B. Goldfarb, IEEE Trans. Magn. **27**, 3601 (1991).

[17]F. Irie, Y. Tsujioka, and T. Chiba, Supercond. Sci. Technol. **5**, S379 (1992).

[18]R. Griessen, Phys. Rev. Lett. **64**, 1674 (1990).

[19]R. Wördenweber and M. O. Abd-El-Hamed, J. Appl. Phys. **71**, 808 (1992).

[20]O. F. Schilling, K. Aihara, and S. Matsuda, Physica C **201**, 397 (1992).

[21]C. J. van der Beek and P. H. Kes, Phys. Rev. B **43**, 13 032 (1991).

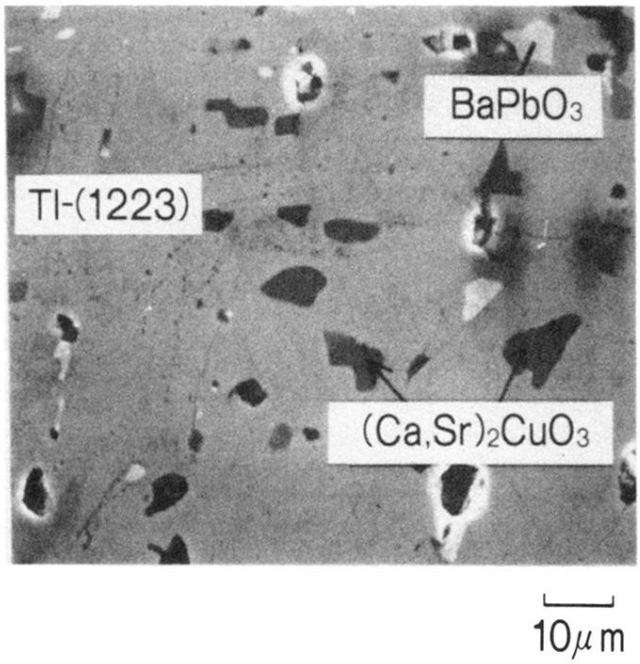

FIG. 1. SEM micrograph showing a large Tl-(1:2:2:3) grain with other phases embedded in it.